Arab J Sci Eng (2014) 39:2097–2106
DOI 10.1007/s13369-013-0754-3

RESEARCH ARTICLE - MECHANICAL ENGINEERING

Ni–WC Coating on AISI 1010 Steel Using TIG: Microstructure and Microhardness

Gul Tosun

Received: 22 March 2012 / Accepted: 13 July 2013 / Published online: 5 September 2013

Abstract In this study, mixed powders of Ni and WC were coated using tungsten inert gas method on the surface of AISI 1010 steel. The effects of current and thickness of the pre-placed powder layer on the microstructure and hardness of the alloyed surfaces were investigated. The hardness of the alloyed surfaces increased and this was attributed to harder phases. Different microstructures were observed depending on the production parameters. The microstructures of the alloyed surfaces consisted of widmanstatten-type ferrite, grain boundary ferrite, acicular ferrite, bainite and a small amount of martensite phase.

Keywords Ni–WC · Coating · Hardness · Microstructure

الخلاصة

تم - في هذه الدراسة - تغليف مساحيق مختلطة من النيكل وكلوريد الخارصين على سطح صلب ايسي 1010 باستخدام طريقة غاز الخارصين الخامل (TIG) ، وحُقق في آثار التيار وسماكة طبقة المسحوق قبل وضعها على البنية المجهرية وصلابة الأسطح المسبوكة ، فازدادت صلابة الأسطح المسبوكة ، ويعزى هذا إلى مراحل أكثر صلادة. وقد لوحظت بُنى مجهرية مختلفة اعتمادا على عوامل الإنتاج. وتتألف البنى المجهرية للأسطح المسبوكة من الفريت من نوع widmanstatten، وفريت حدود الحبوب، وفريت الأسيكولار، وبينايت وكمية صغيرة من مرحلة martensite.

1 Introduction

Low carbon steels are widely used in engineering applications, because of their low cost, good formability and weldability. However, low mechanical properties, hardness and corrosion resistance restrict their widespread use and application. Therefore, coating technology is emerging as a viable technique to alter the properties of the material by natural or artificial deposition of another material on the bulk phase of the solid. Surface modification methods applied by laser, plasma powder spraying and tungsten inert gas (TIG) welding, which are semi-melting methods, are also applied with this aim [1–4]. Deposits of thickness greater than most other methods, typically in the range of a few mm, can be obtained by the TIG process [5]. It is commonly employed in the repair of eroded surfaces in propellers and in dockyards [5]. The alloying method by means of TIG, which is surface modification, is principally a method that was produced by melting the alloy powder or powders having proper composition placed on the substrate material surface. Melting takes place at the same time in both modified coating material and base metal (substrate), which are bonded with each other in a metallurgical way. Fine-grained microstructures which solidify rapidly contain hard carbide phases [2].

TIG can be used to clad and coat the surfaces of steels. Composite coatings have emerged as a viable method by which the wear resistance of the desired engineering materials can be improved. In this study, a mixture of tungsten carbide (WC) and Ti powders was used. Owing to its high hardness (3,000–4,000 HV) and good wear resistance, tungsten carbide (WC) is widely used as a tool or die material [3]. As compared to other carbides, WC combines favorable properties, such as high hardness, a certain amount of plasticity and good wettability by molten metals [6,7]. However, the brittleness of WC precludes its use as a structural material. In addition to promoting the wear performance of the surface, clad tungsten carbide particles on a ductile material possesses the toughness of the substrate [3]. The main disadvantage of WC is its low heat of formation, which makes it easily dissolvable by molten metals, and the brittleness of

G. Tosun (✉)
Metallurgy and Material Engineering Department,
Technology Faculty, Firat University, 23119 Elazig, Turkey
e-mail: gultosun@firat.edu.tr

WC-base composites (cemented carbides) limits their usefulness in certain wear applications where a combination of high hardness and toughness is needed [6].

Buytoz et al. [2] studied dry sliding wear behavior of WC composite coatings on AISI 4340 steel fabricated by TIG process. As a result of microstructure examinations, eutectic and dendrite solidifications were observed together with WC, W_2C phases in the surface modified layers. The hardness values were obtained between 950 and 1,200 HV in the produced layer. Lin and Chang [3] examined the microstructure, hardness and wear behavior of tungsten carbide multipass cladding on AISI 1050 steel by TIG welding process. They reported that the metastable phase in the clad layer could be transferred to stable phase in situ and can cause reduced wear resistance of the multi-pass clad layers. Mridha et al. [8] examined titanium aluminide coatings produced by elemental powders preplacement and TIG surface melting process. They proved that the wear resistance property of the coated layer was about three to four times higher than that of the untreated titanium layer. Wang and Xu [9] examined wear behavior, microhardness and microstructure of nanostructured Ni–WC–Co composite coatings on nickel-plated stainless steel substrates produced by electrophoretic deposition. They observed that the coatings containing nanostructured WC–Co particles showed a significant increase in hardness and wear resistance. Zhong et al. [10] examined the formation of WC/Ni hard alloy coating by laser cladding of W/C/Ni pure element powder blend. They analyzed the dissolution behavior of W and C/Ni clad powders, microstructure and phase of the cladded coatings. The results indicated that the coating contained WC, CW_3, WNi, FeW_3C, Fe_6W_6C, W_3O, W, C and (Fe, Ni) phases. Zhou et al. [11] studied Ni-based WC composite coatings by laser induction hybrid rapid cladding with elliptical spot. Surender et al. [12] investigated the tribological properties of Ni–WC composite coatings electrodeposited on steel substrate. They showed that the addition of WC in Ni increases the microhardness of the coatings. Alian and Jalham [13] performed a comparative work among three different types of coating materials to improve the wear resistance of steel by using a plasma-spray process. They investigated the effect of velocity, load and surface roughness for each coating type.

In this study, the surface of the AISI 1010 steel was coated with preplaced tungsten carbide/nickel powder mixture, using a tungsten arc heat source (torch). To the best of the knowledge of the author of the present work, the literature did not reveal studies on Ni–WC composite coatings of AISI 1010 steel by the TIG process. In addition, this study was performed to expand the usage areas of low carbon steels. Therefore, the effects of the coating thickness and current value on the microstructure and microhardness of coatings were investigated. EDX, XRD and SEM analyses were used to assess the compositions of coating layer.

2 Experimental Procedure

AISI 1010 steel with the dimensions of 100 × 20 × 10 mm was selected as the substrate material.Prior to the cladding process, the substrate was polished with 400 grit SiC emery paper, cleaned and finally rinsed with acetone. The mixed powders of Ni and WC with at 95 % Niand at 5 % WC were blended for 12 h. The characteristic features of powders used are shown in Table 1.

Then the mixed powder layers in thickness of 1 and 2 mm were covered with a paste of the alloying powder by adding pure alcohol so that the powders bind. The binder was restricted within a limit to eliminate pore formation [6] and keep the powders on the surface under the flow of argon during arc melting. The coated specimens were dried in a furnace at 60 °C for 1 h to enhance the adhesion effect between the coating material and substrate. By varying the thickness of the preplaced powder on the surface, different amounts of elements melting in the alloyed zone were controlled. The TIG arc used for the glazing action was produced with an operation current ranging from 100, 120 to 140 A as shown in Fig. 1 [8]. A tungsten electrode of 2 mm diameter was used to produce a stable arc which was controlled by the supply of current and voltage to the electrode. The experimental parameter settings are shown in Table 2.

The hardness measurements were performed on the polished cross sections of the coatings by Leica microhardness tester. Microhardness measurements were carried out using a 200 g load starting from the top to the bottom of the coatings. Specimens for metallographic examinations were taken from cross section of the modified surface from the coating areas. The metallographic specimens obtained were rubbed with 80–1,200 mesh sandpaper; as a result, their surfaces were cleaned and then cross-sectional surfaces were polished by 3 μm diamond paste and solvent. For microstructural examination, the specimens were etched with 2 % nital. Conventional characterization techniques such as optical (CoicXJP-6), scanning electron microscopy (SEM), energy dispersive spectrograph (EDS) (Jeol JSM 7001F) and X-ray diffractometer (XRD) (Bruker D8 Advance) were employed for studying the microstructure and elemental analysis of the alloyed zone.

Table 1 Characteristics of WC and Ni powders

Feature of coating material	Ni	WC
Purity (%)	99.8	99.5
Specific gravity (g/mol)	58.71	47.9
Powder dimension (mesh)	−325	70 μm
Melting temperature (°C)	1,453	2,870
Specific weight (g/cm^3)	8.9	4.507
Boiling temperature (°C)	2,832	6,000

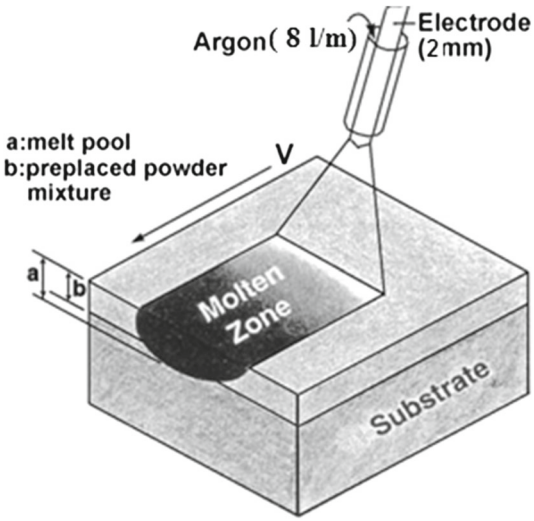

Fig. 1 TIG torch glazing feature [8]

Table 2 The experimental parameters and their values

Parameters	Values
Current, I (A)	100, 120, 140
Coating thickness, t (mm)	1, 2
Scan speed (mm/s)	1.2–1.5
Gas flow rate (l/min)	8
Shielding gas	99.9 % Pure argon
Electrode	2 % Thorium tungsten
Electrode diameter (mm)	2
Voltage (V)	20

3 Results and Discussions

3.1 Microstructure

The arc energy melts the surface of the substrate and the powder layer together and gives an alloyed surface. The elements from the substrate transform the composition and structure of the transition zone in the proximity of the substrate [4]. From the microstructures of the layers cladded with Ni/WC after the TIG process, it was seen that microstructures solidified in varying composition with the process parameters such as coating thickness and energy input values (Figs. 2, 3, 4, 5, 6, 7, 8, 9). The increasing operation current increases both the energy density of torch and heat input for stable voltage [1]. Heat input (energy input) can be calculated using the following equation [14]:

$$\text{Heat inputs} = (\text{current} \times \text{voltage} \times 0.48)/\text{travel speed} \quad (1)$$

A weldment basically consists of four microstructurally distinct regions normally identified as fusion zone, unmixed region, partially melted region, HAZ (Heat affected zone), and unaffected base metal (substrate). This can be seen in Fig. 2. Every point of the weldment in the HAZ relative to the fusion line is subjected to a thermal cycle between maximum temperature and cooling rate during welding [4]. During the coating process, liquation can be seen along the grain boundary in a region very close to the fusion boundary. Probably, liquation is followed by solidification in both the directions parallel and perpendicular to the heat flow [15]. An alloyed layer joined as a result of the melting of a thin layer of the substrate material. The melting points of both W and C are over 3,000 °C, but the temperature of a TIG-induced melt pool during cladding is usually less than 3,000 °C, Therefore, WC is not fully melted directly, but dissolved into the melt pool [10]. However, Ni having a lower melting temperature in the powder blend is well melted into the melt pool. Less than half of the heat generated in a TIG welding arc is transferred to the workpiece (anode) [16]. Therefore we do not expect all the nickel to vaporize and the existence of nickel was shown by EDS analysis (Fig. 4). The dissolution extent depends on the temperature and the duration of the melt pool. In a rapid heating and cooling process at different temperatures, the dissolution of both graphite and tungsten powders may not be totally complete and give different morphologies [10].

A clear metallurgical band was seen in the boundary area between the cladded layer and the substrate in Fig. 2. There is a transition zone at the interface between the coating and the substrate, while more WC particles existed along the coating to the substrate [7]. The cladded part is composed of incompletely melted tungsten/WC particles and the solidification structure with a mixed composition of cladding powder blend and substrate, whereas the substrate side is the heat-treated structure of 1010 steel. The dark-colored particles in Fig. 3 are the partly dissolved WC powder particles. Its EDX analysis is seen in Fig. 4. More particles were seen in the sides and bottom of each layer due to their higher density (Fig. 3).

In coating, a heterogeneous distribution of WC particles, with good interfacial bonding between the particle phase and the matrix, was observed. Cracking, pore and other defects were not observed [7]. A microstructure without crack, pore and other defects indicates good interfacial bonding. Some relatively larger powders cannot melt completely and remain in the coating, especially in the bottom and side area where the temperature is lower than the middle. The incomplete dissolution of tungsten powders influences the composition of the melt. WC particles tend to sink to the bottom of the melt pool due to the great difference in the powder density between WC and Ni. The lower melting points and slower solidification rates of the Ni allow time for the WC particles to sink towards the bottom of the melt pool (Fig. 2). The dominant phases in the microstructure of the substrate material are martensite and bainite. Depending on the rate of

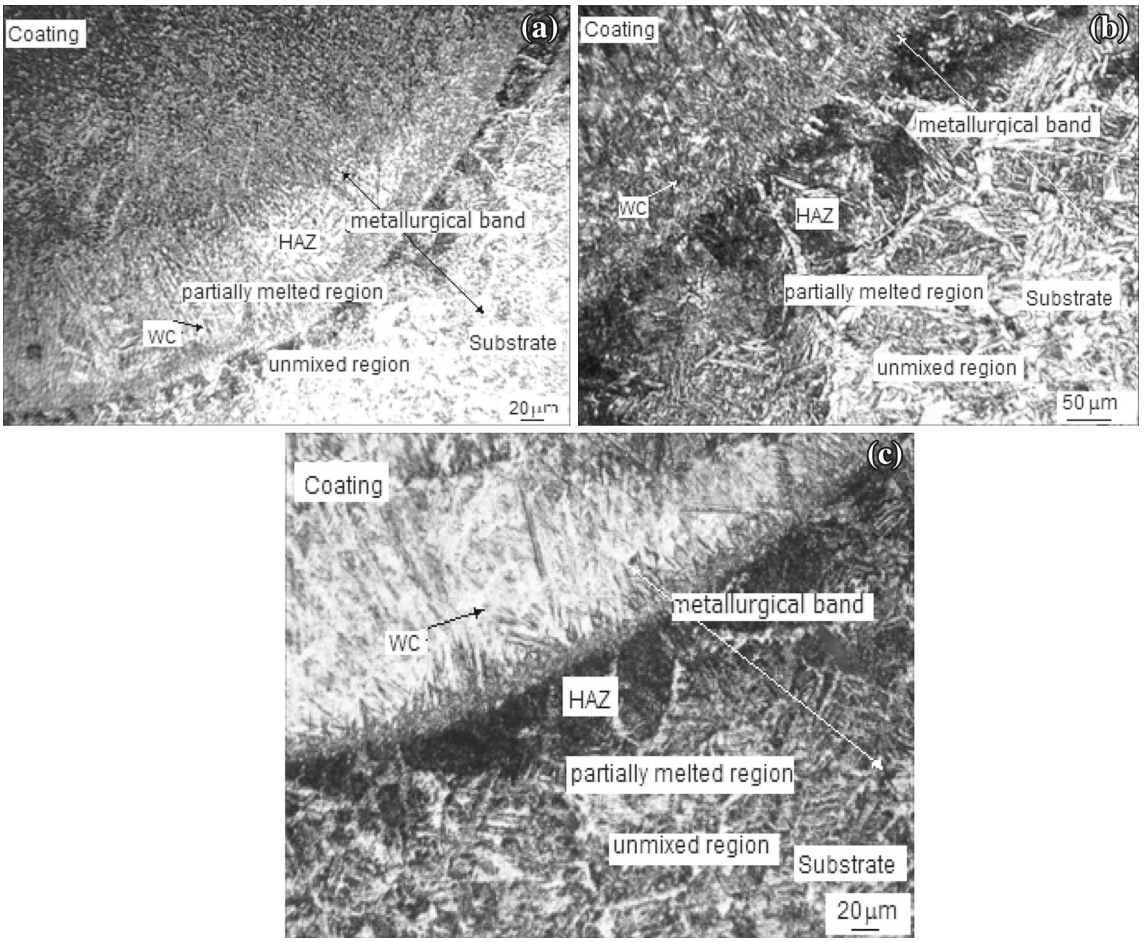

Fig. 2 Optical micrograph of the specimen alloyed with t = 1 mm. **a** I = 100 A, **b** I = 120 A, **c** I = 140 A

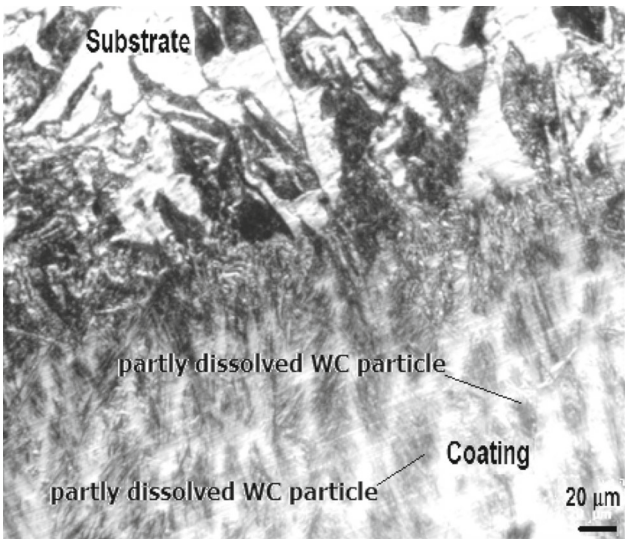

Fig. 3 Optical micrograph of the incompletely dissolved WC powder particles in coating

cooling, it was observed that grain boundary ferrite (GBF), widmanstatten-type ferrite (WF), acicular (needlike) ferrite (AF) and a very small amount of martensite with austenite and decomposed pearlite phase occurred (Figs. 5, 6). In low carbon steels, it is not required that the presence of WF and GBF causes grain coarsening in HAZ. The presence of GBF which depends on the amount of WF is the reason for the loss of toughness and brittle cracking in the weld. The nucleation of AF, usually due to non-metallic inclusions, improves the material toughness and strength. The bainite microstructure in steel with low carbon is very similar to that of AF and therefore it is very difficult to determine these phases [17].

In Fig. 2, it was observed in samples using the same quantities of powder rate and different heat input values that the microstructure changed when the production parameters changed. It was seen that the heat input acted on the microstructures of the alloyed surfaces. In other words, the coating material exhibited a different microstructure after solidification, depending on the heat input value [2].

Considering the W–Fe–C phase diagram, it is possible to say that WC + α-Fe + hexagonal (M_6C) phases may be formed. In the microstructure of the surface modified material, WC and W_2C types, most of which were M_6C (M = W, Fe) carbides (Fig. 4), were determined together with austenitic hypoeutectic structure [2]. The formation of

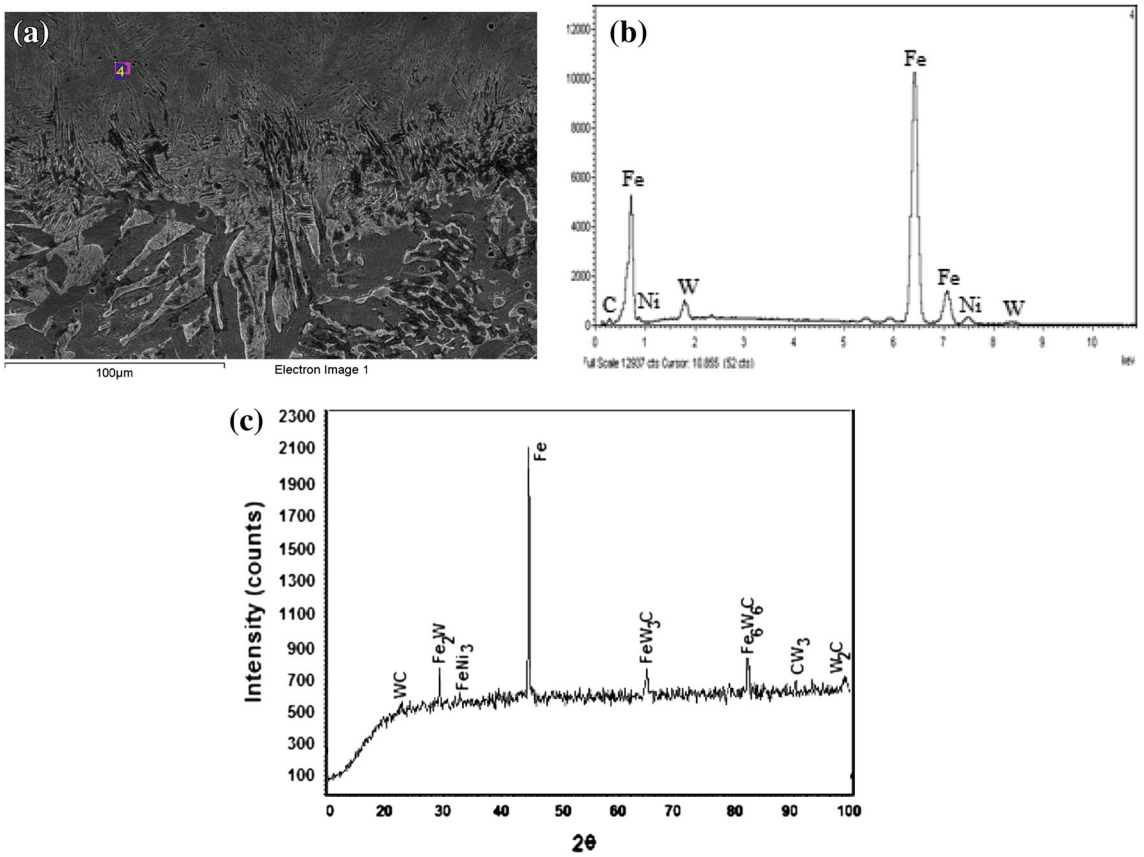

Fig. 4 **a** SEM micrograph of the specimen alloyed with $t = 1$ mm, $I = 100$ A. **b** EDS analysis taken on the point of number 4. **c** X-Ray diffractograms

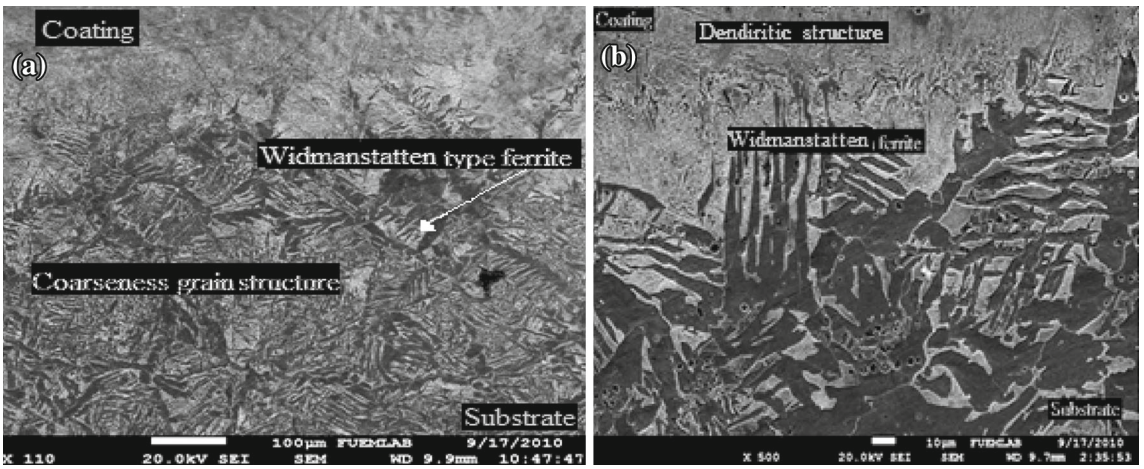

Fig. 5 SEM micrograph of the specimen alloyed with $t = 1$ mm: **a** $I = 120$ A, **b** $I = 140$ A

FeW_3C and Fe_6W_6C in Fig. 4 indicates the significance of even a small amount of melted iron from the substrate in the microstructure of the coating.

In the samples having a coated layer of 1 mm, a slower solidification occurs with heat input increase. The melting efficiency of TIG welding increases with the increasing current intensity [18]. Therefore, when the heat input increased, it was observed that both a small amount of widmanstatten-type ferrite and grain coarsening occurred in HAZ (Fig. 5). In addition, it was observed on the coating side of HAZ that dendritic structures began to form due to the presence of alloy elements (Fig. 5b). The dendritic structures occur perpendicular to the welding axis. It reveals that the dendrites are generally coarser near the coating layer/substrate material inter-

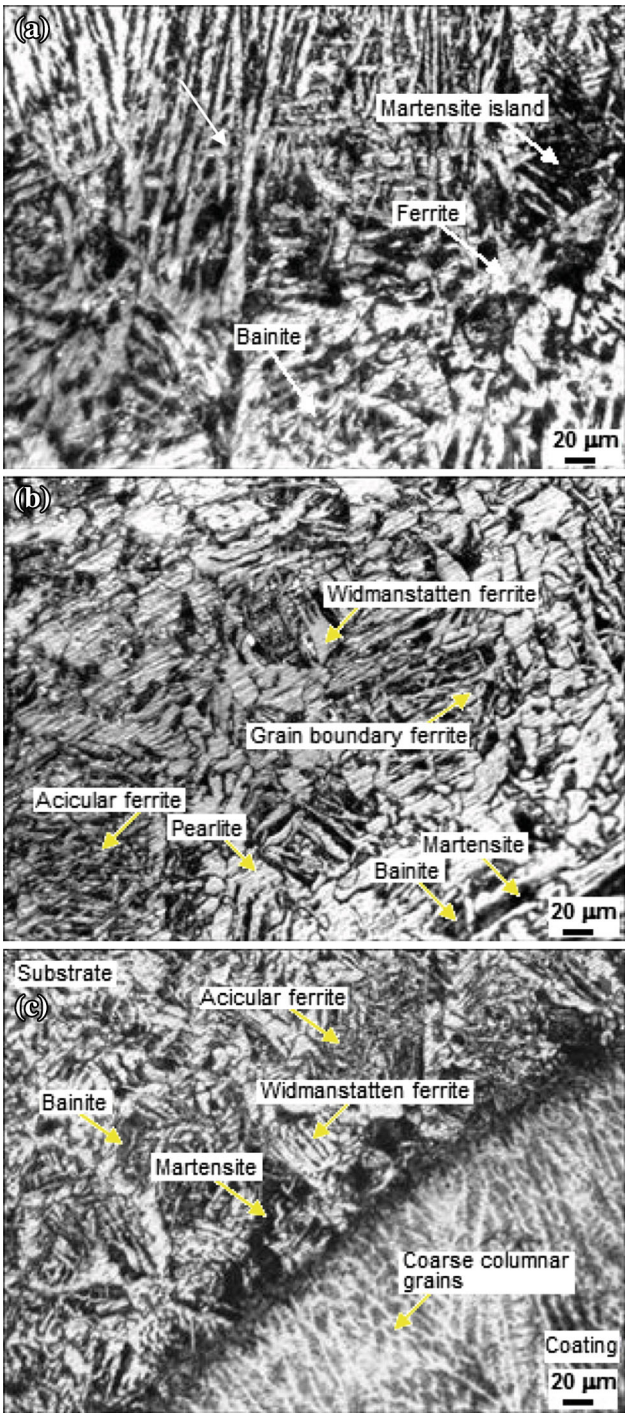

Fig. 6 Optical micrograph of HAZ microstructure: **a** t = 2 mm, I = 100 A, **b** t = 2 mm, I = 140 A, **c** t = 1 mm, I = 100 A

face and dispersed in the matrix. Grain structure at the fusion boundary is very coarse and columnar showing that epitaxial growth has taken place (Fig. 6) [17]. A reason for obtaining the dendritic structure is the large difference between the melting points of Ni and other phases formed by tungsten carbide dissolution. Increasing heat input to the weld metal causes longer solidification time for the melt metal [19].

The energy input of the material is minimum in low current value. It means a high cooling rate, which is concluded by rapid solidification. A small amount of alloying elements in the melt pool was included in the main material; therefore a narrower HAZ and low penetration occurred. As a result, the martensite phase occurs. Martensite islands occurred along the grain boundaries and surrounded by ferrite grains were seen in Fig. 6a. There are similar results in literature [2]. The amount of W in the dendrites was low. Since dendrites are the first to be solidified, the extra W in the melt generally solidifies in only eutectic areas. The WC grains normally melt and dissolve in the melt bath again. During the cooling, WC particles partly dissociated at the edge, and needle-like dendrites grew epitaxially from the surface of the partially melted WC particles. This can harden the matrix and also cause the gradient transition from the matrix to WC hard phases [7].

When proceeded at a low energy density (100 A) for the specimen alloyed with a 2 mm-thick Ni/WC layer (Fig. 6a), the melting occurred mostly onto the precoated powder mixtures and formed a thin layer of the melt pool. As the thickness of the alloyed surface directly depends on the increase of the powder layer, both the amount of elements in the alloyed surface from the powder layer and the content of the carbon in the alloyed zone increase. Larger martensite islands that occurred along the grain boundaries prove this (Fig. 6a, c). The carbon-rich austenite turns into martensite with high carbon and bainite, while the carbon-poor austenite turns into ferrite (Fig. 7) [20]. Principally, the heat input given by the tungsten electrode at relatively high powder contents is absorbed with the alloy powder, reducing the extent of substrate melting [11].

With the current intensity increase, needle like Ni/WC alloy was transformed inti a spherical-shaped grain structure in coating (Fig. 8). On considering that a higher heat input is effective on a lower cooling rate, which causes higher temperature transformation products, such as pearlite (Fig. 9), the results obtained from the surfaces alloyed are in good agreement with the literature [14]. Furthermore, the formation of pearlite with cementite instead of martensite in substrate can be directly attributed to the high heat input used for arc melting. In addition, high heat input and powder content cause formation of the refined dendrites and interdendritic eutectic structure (Fig. 9). Figure 6b shows that Widmanstatten ferrite plates developed from prior austenite grain boundaries in the alloyed surface white areas. The austenite matrix subsequently transformed to pearlite on cooling. Processing with high energy density arcs created complete melting of the powder layer, and the solidified microstructure consisted of lamellar and Widmanstatten-type structure [8]. The interface thickness plays a key role in determining whether Widmanstatten growth is possible or not [21]. Increase in the amount of WC was found to be parallel to that of the dendrite

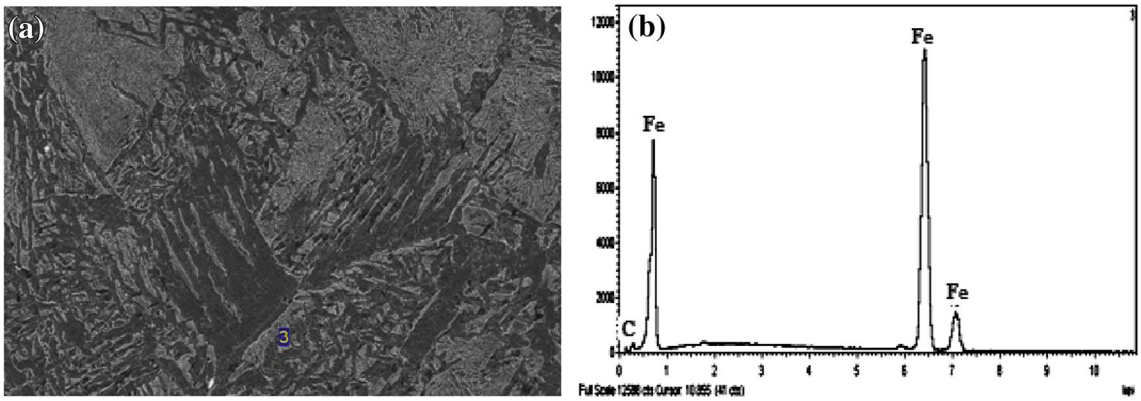

Fig. 7 **a** SEM micrograph of the HAZ of specimen alloyed with $t = 2$ mm, $I = 120$ A. **b** EDS analysis taken on the point of number 3

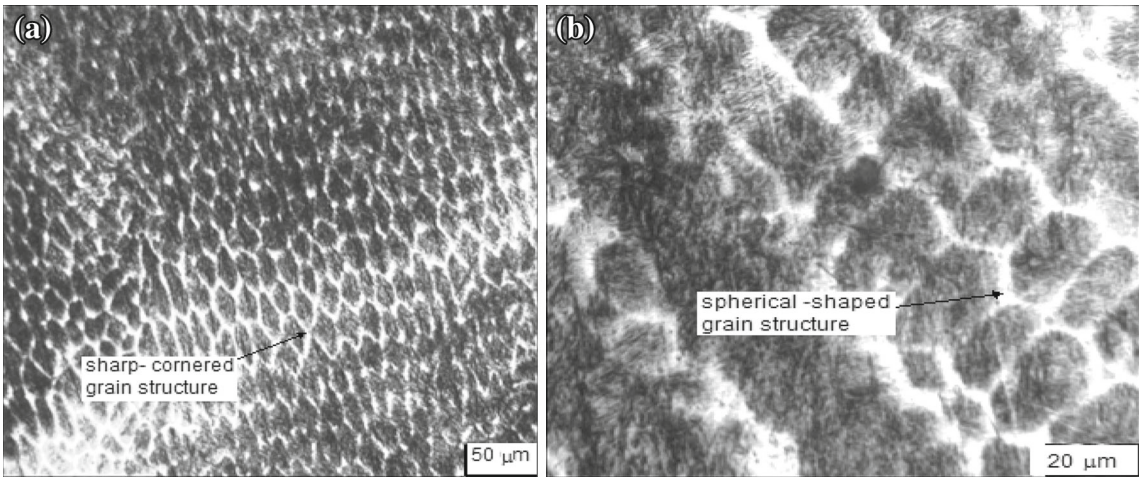

Fig. 8 Optical micrograph of the coating in the specimen alloyed with $t = 1$ mm, $I = 140$ A

formation amount (Fig. 6a). When the structure is supersaturated with respect to temperature and C content, Widmanstatten plates begin to grow [21]. As a result, when current was increased, both Widmanstatten-type structure was seen in HAZ (Fig. 6b) and grain structure coarsening occurred. Consequently, the width of HAZ increased. Additionally, it was observed that grain boundary ferrite, acicular ferrite, bainite and a small amount of martensite phase occurred in the microstructure (Fig. 6b).

3.2 Microhardness

The effect of current density on the microhardness of the composite layer and variation in microhardness as a function of coating thickness in the composite coated layer are shown in Fig. 10. It was seen in Fig. 10 that the hardness of the coating layer increased with the increase in the current. High current is known to increase heat input and to cause the lower cooling rate encountered by the weld pool. Low cooling rate allows the grain to grow to a large extent due to longer solidification time and thereby coarsen the structure. Microhardness appears to be closely related to the microstructure. In general, refinement of grain structure showed improvement in the hardness. The grain structure coarsens with an increase in the peak current [20]. When current is increased, it is expected to decrease the hardness due to grain coarsening with a 1 mm-thick Ni/WC coating. On the contrary, a spectacular increase in the hardness of the coating is observed. This can be simply attributed to WF, AF and some bainite formation and to the spectacular high carbon content of this region [17]. In addition, the high hardness of WC and W_2C-type carbides concentrated in high-dendritic structure increased hardness of the samples at the highest current (140 A) and 1 mm-thick Ni/WC coating (Fig. 6). In a 2 mm-thick Ni/WC coating, when current increased, hardness also increased due to pearlite occurring with cementite.The main body of dendrites coarsened with the increase in the current (Fig. 2). The results in Fig. 10 and Fig. 2a showed that the hardness of the coating layer linearly depended on the coating thickness [22]. The presence of the WC and W_6C-type carbides in the coarsening dendrites caused the highest hardness. The increase in

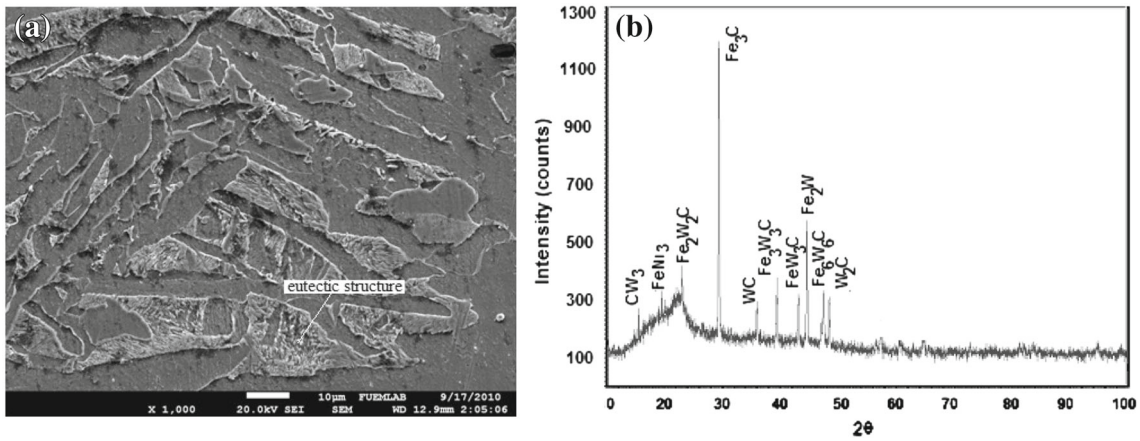

Fig. 9 The coating of the specimen alloyed with $t = 2$ mm, $I = 140$ A. **a** SEM micrograph. **b** X-Ray diffractograms

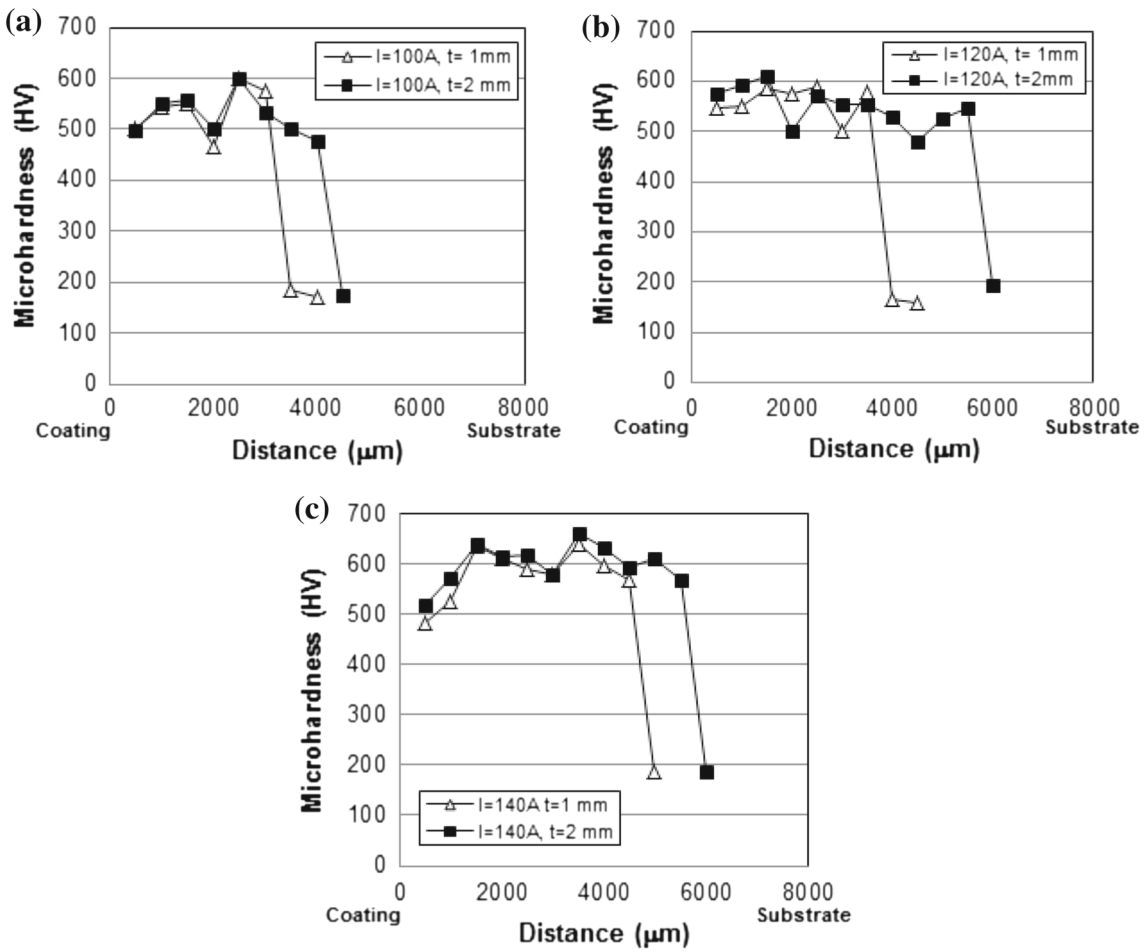

Fig. 10 Effect of coating thickness on the microhardness

microhardness is due to the fast cooling rate experienced near the weld area, which produces a supersaturated solid solution in HAZ.

The hardness values of the samples varied between 160 and 660 HV. The hardness values of the coating layers in 100, 120 and 140 A currents varied between 467–600, 479–610 and 482–660 HV, respectively. The alloyed layer developed hardness of three to four times the base hardness. The highest hardness value in the coatings was obtained in 140 A current value as 660 HV. Therefore the microstructural character-

istics of the hardfacing specimens are strongly dependent on heat input values as well, which in turn results in different microstructures [23]. Peak hardness is somewhere in the middle of the coating. Fluctuations in the hardness values of coating layer might be due to the variation of chemical composition of the coating across the interface. Increase in microhardness with distance from the interface may be attributed to the increased fraction of hard carbide particles away from the interface. Low hardness near the interface may be due to decarburization of the alloy elements during alloying [1]. The hardness values in HAZ were higher than the values of the substrate material. It was observed that grain structures of particles are coarse and larger in the optical microstructure image of HAZ in Fig. 6 [17]. Furthermore, the interfacial bond between the substrate and the coating occurring with the formation of this region increases. This is undesirable.

The microhardness of the matrix of the composite coating increased with increasing amount of WC particles in the composite coating [1,12]. When the powder feed quantity on the material surface increased, the percentage rates of the W, C and Ni elements increased compared to the chemical concentration of AISI 1010 steel. The hardness increase noted in these composite coatings could be linked to a dispersion-strengthening effect [12]. When the carbide content increased, the hardness of the coating layer increased (Fig. 10). In general, the results of the hardness measurement are in good agreement with literature.

4 Conclusions

The following conclusions were derived from the surface modification with Ni/WC using the TIG method.

- A clear metallurgical bonding between the cladded layer and the substrate was observed.
- In coating, a heterogeneous distribution of WC particles with good interfacial bonding between the particle phase and the matrix was observed and no cracking occurred. Widmanstatten ferrite and grain coarsening formed in the substrate or in the HAZ.
- In low coating thickness (1 mm), when the heat input increased, both formation of a small amount of widmanstatten-type ferrite and grain coarsening occurred. Some relatively larger WC powders cannot melt completely and remain in the coating, especially in the bottom and side area where the temperature is lower than the middle.
- Locations with high coating thickness (2 mm) are where these martensite and ferrite structures are seen. When low current was selected, it was seen that martensite islands occurred along the grain boundary and were surrounded by ferrite grains. As current is increased, widmanstatten-type ferrite increases. When current is increased, both widmanstatten-type perlite, grain boundary ferrite, acicular ferrite, bainite and a small amount of martensite phase are seen in HAZ and the grain structure becomes coarse.
- When current is increased, the microhardness of the composite coating increases.
- The microhardness of the matrix of the composite coating increased with increasing amount of WC particles in the composite coating.

As a result, in the microstructure of the material with the WC modification, depending on the heat input, two significant solidification characteristics were found.

References

1. Harsha, S.; Dwivedi, D.K.; Agarwal, A.: Influence of CrC addition in Ni–Cr–Si–B flame sprayed coatings on microstructure, microhardness and wear behaviour. Int. J. Adv. Manuf. Tech. **38**, 93–101 (2008)
2. Buytoz, S.; Ulutan, M.; Yildirim, M.M.: Dry sliding wear behavior of TIG welding clad WC composite coatings. Appl. Surf. Sci. **252**, 1313–1323 (2005)
3. Lin, Y.C.; Chang, K.Y.: Elucidating the microstructure and wear behavior of tungsten carbide multi-pass cladding on AISI 1050 steel. J. Mater. Process Technol. **210**, 219–225 (2010)
4. Eroglu, M.: Boride coatings on steel using shielded metal arc welding electrode: microstructure and hardness. Surf. Coat. Technol. **203**, 2229–2235 (2009)
5. Cheng, F.T.; Lo, K.H.; Man, H.C.: NiTi cladding on stainless steel by TIG surfacing process Part I. Cavitation erosion behavior. Surf. Coat. Technol. **172**, 308–315 (2003)
6. Lou, D.; Hellman, J.; Luhulima, D.; Liimatainen, J.; Lindroos, V.K.: Interactions between tungsten carbide (WC) particulates and metal matrix in WC-reinforced composites. Mater. Sci. Eng. A Struct. **340**, 155–162 (2003)
7. Wu, P.; Du, H.M.; Chen, X.L.; Li, Z.Q.; Bai H.L.; Jiang, E.Y.: Influence of WC particle behavior on the wear resistance properties of Ni–WC composite coatings. Wear **257**, 142–147 (2004)
8. Mridha, S.; Ong, H.S.; Poh, L.S.; Cheang, P.: Intermetallic coatings produced by TIG surface melting. J. Mater. Process Technol. **113**, 516–520 (2001)
9. Wang, Y.; Xu, Z.: Nanostructured Ni–WC–Co composite coatings fabricated by electrophoretic deposition. Surf. Coat. Technol. **200**, 3896–3902 (2006)
10. Zhong, M.; Liu, W.; Zhang, Y.; Zhu, X.: Formation of WC/Ni hard alloy coating by laser cladding of W/C/Ni pure element powder blend. Int. J. Refract. Metals Hard Mater. **24**, 453–460 (2006)
11. Zhou, S.; Huang, Y.; Zeng, X.: A study of Ni-based WC composite coatings by laser induction hybrid rapid cladding with elliptical spot. Appl. Surf. Sci. **254**, 3110–3119 (2008)
12. Surender, M.; Basu, B.; Balasubramaniam, R.: Wear characterization of electrodeposited Ni–WC composite coatings. Tribol. Int. **37**, 743–749 (2004)
13. Alian, A.; Jalham, I.S.: Abrasive wear resistance comparative study of plasma- sprayed steel by magnesium zirconate, aluminum-bronze, molybdenum, and mixtures of them as coating materials. Arab. J. Sci. Eng. **31**(1B), 27–34 (2006)
14. Eroglu, M.; Ozdemir, N.: Tungsten-inert gas surface alloying of a low carbon steel. Surf. Coat. Technol. **154**, 209–217 (2002)

15. Manti, R.; Dwivedi, D.K.; Agarwal, A.: Microstructure and hardness of Al–Mg–Si weldments produced by pulse GTA welding. Int. J. Adv. Manuf. Technol. **36**, 263–269 (2008)
16. Quigley, M.B.C.; Richards, P.H.; Swift-Hook, D.T.; Gick, A.E.F.: Heat flow to the workpiece from a TIG welding arc. J. Phys. D Appl. Phys. **6**, 2250–2259 (1973)
17. Gural, A.; Bostan, B.; Ozdemir, A.T.: Heat treatment in two phase region and its effect on microstructure and mechanical strength after welding of a low carbon steel. Mater. Design **28**, 897–903 (2007)
18. Tusek, J.; Suban, M.: Hydrogen Energy Experimental research of the effect of hydrogen in argon as a shielding gas in arc welding of high-alloy stainless steel. Int. J. Hydrogen Energy **25**, 369–376 (2000)
19. Durgutlu, A.: Experimental investigation of the effect of hydrogen in argon as a shielding gas on TIG welding of austenitic stainless steel. Mater. Design **25**, 19–23 (2004)
20. Eroglu, M.; Aksoy M.; Orhan, N.: Effect of coarse initial grain size on microstructure and mechanical properties of weld metal and HAZ of a low carbon steel. Mater. Sci. Eng. A Struct. **269** 59–66 (1999)
21. Loginova, I.; Agren, J.; Amberg, G.: On the formation of Widmansttatten ferrite in binary Fe–C–phasefield approach. Acta Mater. **52**, 4055–4063 (2004)
22. Van Acker, K.; Vanhoyweghen, D.; Persoons, R.; Vangrunderbeek, J.: Influence of tungsten carbide particle size and distribution on the wear resistance of laser clad WC/Ni coatings, Wear **258**, 194–202 (2005)
23. Buytoz, S.; Ulutan, M.: In situ synthesis of SiC reinforced MMC surface on AISI 304 stainless steel by TIG surface alloying. Surf. Coat. Technol. **200**, 3698–3704 (2006)